LAWRENCE
LIVERMORE
NATIONAL
LABORATORY

LLNL-JRNL-407959

Line Edge Detection and Characterization in SEM Images using Wavelets

W. Sun, J. A. Romagnoli, J. W. Tringe, S. E. Létant, P. Stroeve, A. Palazoglu

October 21, 2008

Institute of Electrical and Electronics Engineers Transactions on Semiconductor Manufacturing

Disclaimer

Line Edge Detection and Characterization in SEM Images using Wavelets

Wei Sun, Jose A. Romagnoli, Joseph W. Tringe, *Member, IEEE*, Sonia E. Létant, Pieter Stroeve and Ahmet Palazoglu

***Abstract*—Edge characterization has become increasingly important in nanotechnology due to the growing demand for precise nanoscale structure fabrication and assembly. Edge detection is often performed by thresholding the spatial information of a top-down image obtained by Scanning Electron Microscopy (SEM) or other surface characterization techniques. Results are highly dependent on an arbitrary threshold value, which makes it difficult to reveal the nature of the real surface and to compare results among images. In this paper, we present an alternative edge boundary detection technique based on the wavelet framework. Our results indicate that the method facilitates nano-scale edge detection and characterization, by providing a systematic threshold determination step.**

***Index Terms*—Line Edge Roughness (LER), SEM, wavelets.**

I. Introduction

Line edge characterization is a bridge connecting the performance of a device with the fabrication process. It provides a practical metric that can improve single device performance and reduce device-to-device variability [1], [2]. Yamaguchi et al. [2], for example, recently described a new process for defining line edge roughness (LER) appropriately for next-generation transistors, and for defining a target roughness value for meeting device performance targets. The determination of LER in a structure, however, requires a first critical measurement step to *recognize* these edges in an image: identifying the location of the boundaries, for example in units of pixels or nanometers. Historically, the recognition of line edges has been a subjective, variable process. Here, we introduce a new process which employs the wavelet transform to create a deterministic, image-based definition of this critical quantity.

There are several line edge characterization methods described in the literature [4] but the first step in this effort is always 'edge identification' that uses images taken from the real surface, which usually are top-down SEM or Atomic Force Microscopy (AFM) images. As expected, edge roughness characterization is highly dependent on the imaging method and also on the edge boundary detected. Since all imaging methods carry various degrees of noise that masks the real surface features and patterns, it becomes crucial for a characterization method to uncover the surface structure and to allow detection of the real edge boundary.

In practice, it is difficult to unequivocally differentiate the signal contributions that originate from the imaging process from the ones that correspond to the real surface in the spatial domain. A recent computational technique, the wavelet decomposition [5], makes it possible to observe a given signal (image) at different resolutions or frequencies that correspond to different topographical features, such as underlying peaks and valleys, or detailed variations on a surface. This facilitates the detection and isolation of random surface features and noise from the relevant ones and can form the basis of subsequent quantitative analysis steps. We have shown previously that wavelet decomposition can help in extracting specific image features from AFM images and allow them to be studied in detail [6]. Wavelet decomposition was previously used in SEM image processing [7], [8] in the context of fault detection in the etching process. More recently, wavelets have been used for the estimation of the electron probe profile from SEM images [9].

In this paper, a wavelet-based method for edge detection in SEM images is proposed and its performance is compared with an existing method. With the new method, image enhancement is performed by intensity normalization and then the image is de-noised first, similar to existing practice. This step is followed, however, by wavelet decomposition to specify edge and background levels so that LER characterization can be rigorously performed. We show that the wavelet-based edge detection strategy can yield an image-dependent edge boundary to facilitate edge roughness characterization. This provides a systematic evaluation of the

Manuscript submitted February 27, 2008. This work was performed under the auspices of the U.S. Department of Energy by Lawrence Livermore National Laboratory under Contract DE-AC52-07NA27344.

W. Sun is with the Beijing University of Chemical Technology, Beijing, China (e-mail: sunwei@mail.buct.edu.cn).

J. A. Romagnoli is with the Cain Department of Chemical Engineering, Louisiana State University, Baton Rouge, LA 70803-7303 USA (e-mail: jose@lsu.edu).

J. W. Tringe is with the Chemistry, Materials, Earth and Life Science Directorate, Lawrence Livermore National Laboratory, Livermore, CA 94551-9900 USA (e-mail: tringe2@llnl.gov).

S. E. Létant is with the Chemistry, Materials, Earth and Life Science Directorate, Lawrence Livermore National Laboratory, Livermore, CA 94551-9900 USA (e-mail: letant1@llnl.gov).

P. Stroeve is with Department of Chemical Engineering and Materials Science, University of California Davis, Davis, CA 95616 USA (e-mail: pstroeve@ucdavis.edu).

A. Palazoglu is with Department of Chemical Engineering and Materials Science, University of California Davis, Davis, CA 95616 USA (phone: 530-752-8774; fax: 530-752-1031; e-mail: anpalazoglu@ucdavis.edu).

superimposed edge search region and the associated threshold value, which are only properties of the image itself.

II. Edge Detection and Characterization

A. Edge Detection

Edge detection means obtaining the boundaries for a given edge in terms of pixels or nanometer location in an image. Edge characterization is subsequently based on the boundaries found by this edge detection step. The most commonly used approaches for edge detection are signal-threshold and derivative-threshold methods based on a de-noised image [4]. Following image transformation to pixels, de-noising and differentiation, the user needs to make two decisions: (i) how to specify the image region for line edge search, and (ii) how to choose the threshold for boundary detection. The first decision defines the search range in the image, and is often based on a visual observation, which can include all possible regions to avoid losing any critical information for the edge detection step. The second decision is also made visually based on the height or intensity information from an image, which makes line edge roughness characterization depend on the choice of the threshold value. Between these two decisions, one also performs normalization in terms of the intensity value, which is expected to enhance the contrast of the whole image, but will not change the edge boundaries in terms of number of pixels or nanometer location. In this paper, we focus our discussion on the decision that involves the selection of the search region and the threshold to show how such a selection influences edge detection of the resist line and we offer an analytical method to determine it.

B. Edge Characterization

In edge characterization, LER denotes the deviation from a reference straight line or from a reference flat surface depending on if one works in one or two dimensions [1], [2]. Thus, LER can capture two aspects of roughness according to the dimension considered. For surfaces, roughness is based on the height information within the edge, and requires that the image is taken in terms of height. For lines, the edge boundary roughness is based on the boundary location either in terms of number of pixels or nanometer measurement. In this paper, we focus on the latter, since an SEM image is used and edge boundary deviation is more important in this case. Nevertheless, all characterization techniques rely on the edge boundary defined in the edge detection step, hence the conclusions drawn should be valid generally.

There are several ways to characterize the LER. The *sigma* value is chosen in this paper, since it is the most straightforward and most closely related to the line boundary. It is defined as:

$$\sigma = \sqrt{\frac{\sum_{i=1}^{N_p} \delta_i^2}{N_p}} \qquad (1)$$

where N_p is the number of points along the line edge, and δ is the signed distance of each edge point from the linear fit to the line edge [4], [10]. Spatial correlation is also considered as a characterization method in the literature [11], [12].

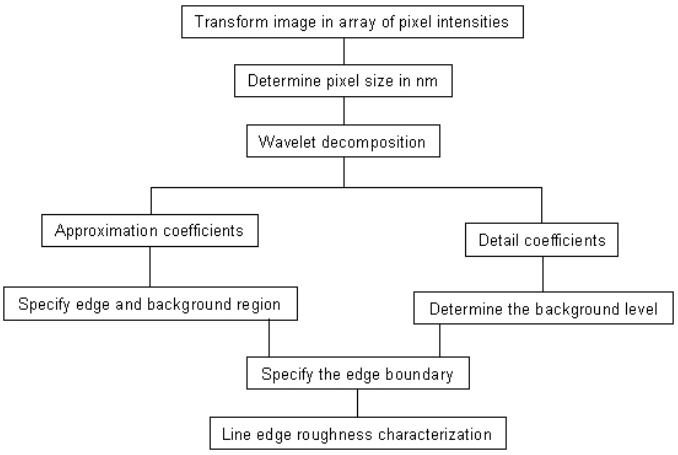

Fig.1. Flowchart of wavelet-based edge detection strategy.

Based on the edge boundary information, correlation between two boundaries for each single edge and maximum intensity lines for a pair of edges are also calculated. This can help quantify the presence (or lack thereof) of synchronization between two boundaries, which could reflect photoresist variations due to, for example, swelling [13], or could reflect charging effects in the SEM during imaging. Edge width variation along the edge distance can also capture the uniformity of an edge [10]. The width information at different threshold values is also discussed in this paper.

III. Wavelet-Based Edge Detection

Wavelet decomposition is widely used in time series and image analysis [5], [14]. Its salient advantage over other analysis methods, especially Fourier transform, is that it can give not only frequency information of a signal, but can also localize that information in the temporal (spatial) domain. The details of the wavelet decomposition are given in the Appendix.

The wavelet-based edge detection strategy is depicted in Figure 1. When an original image is decomposed into the n^{th} level using wavelets, one smoothed (approximation) sub-image and 3n detail sub-images are obtained. The smoothed sub-image reveals the underlying structure of the surface by eliminating imaging noise and the high-frequency details of the surface. By searching the smoothed image, background and edge regions can be defined without the interference of high-frequency components. This step corresponds to the first decision associated with 'the specification of the image region for line edge search' in the conventional edge detection and characterization method, and avoids any input from visual observation. High-frequency sub-images represent the surface deviation of both peaks and valleys, which can be used to define the background intensity and further to determine the intensity level or height value where the edge boundary is located.

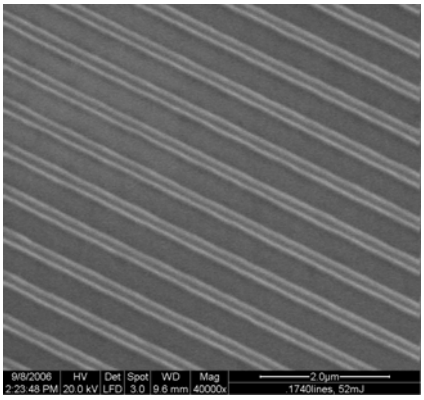

(a)

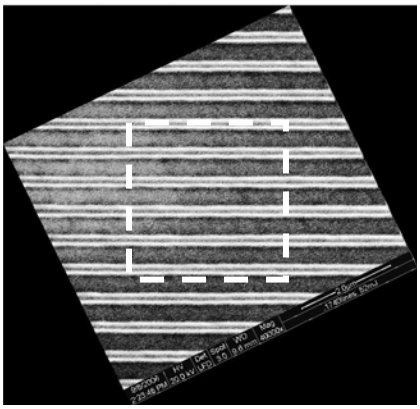

(b)

Fig.2. SEM image from photoresist process, (a) original image, (b) after intensity normalization, rotation and selection of 512×512 image.

The threshold value will influence the edge boundary detection and, in turn, the edge characterization. A suitable threshold value for edge boundary detection is required to separate adjacent edges and retain edge roughness information at the same time. The approximation sub-image describes the underlying surface and yields an average intensity (height level) along the edge separating line. Furthermore, the detail sub-images contain all high-frequency components which represent the deviation of intensity (or height). By combining both the approximation average and the standard deviation of surface details, an image-dependent threshold value can be obtained.

IV. Results and Discussion

A. SEM Image used for Edge Detection and Characterization

An SEM image (Fig. 2a) is used as an example to compare two methods of line edge detection and roughness characterization. The SEM image analyzed is a of a 1740 line/mm plane diffraction grating holographically produced on a 50 mm diameter fused silica substrate. The grating lines are in photoresist, nominally 550 nm tall and 150 nm wide, with nominally vertical sidewalls. High-frequency components may be caused by the photoresist itself or exposure variations, or may be related to the charging process associated with SEM imaging. In this paper, our focus is to characterize the uniformity of the edge and its deviation from the ideal straight line. Characterizing edge uniformity in this consistent manner will help identify sources of variations, whether physically associated with the structure under study, or else related to the imaging process.

The image data are in *tiff* format and imported into MATLAB® to yield an $N \times M$ array for further processing. To increase the contrast of the image, image enhancement was performed by intensity normalization [4]. To avoid artifacts associated with features aligned to the SEM electron beam scanning direction, the scanning direction was not chosen to be parallel to the photoresist lines. To simplify the calculations, however, the image was first rotated to position the image edge horizontally with respect to the photoresist lines, and for subsequent analyses, a 512×512 image was selected (Fig. 2b).

B. Edge Detection by Thresholding and LER Characterization

According to the procedure proposed in [4], the image is first de-noised and normalized in terms of intensity or height. To demonstrate the effectiveness of the edge detection step within the pre-defined edge-search region, we compare edge search results from several threshold values. In this section, the edge-search region is specified visually. Figure 3 shows, for three values of the chosen intensity threshold, how the edge characterization results can vary. Each plot includes the upper and lower edge boundaries and the maximum intensity line as well as the edge width along the edge distance. Figure 3a shows that two adjacent edges are not totally separated when the threshold value is 0.2, since there are several parts of the inner boundary (which corresponds to the upper boundary in Fig. 3a) are straight. The LER based on this boundary cannot reveal the edge characteristics, because no surface roughness exists under that threshold value. As the threshold value increases, edges appear to be well separated and defined, as roughness is revealed along the upper boundary range, but it is also observed that the edge boundaries are smoothed due to the de-noising operation on the intensity direction. This represents the key trade-off in this approach.

A sigma value is calculated from Eq. 1, based on the linear fitting of two boundaries of an edge, revealing the edge roughness at a certain threshold value of intensity. The correlation coefficient between the edge boundaries for each case is also calculated, and can range from -1 to 1. Here, -1 and +1 indicate negative (inverse) and positive (proportional) relationships between the two data sets, respectively, and 0 means that they are independent. Here, we chose to use the absolute value of the correlation coefficient, as we are chiefly interested in the magnitude of correlation, not necessarily its direction. In practice, the correlation coefficient is expected to be small for undamaged photoresist features [10].

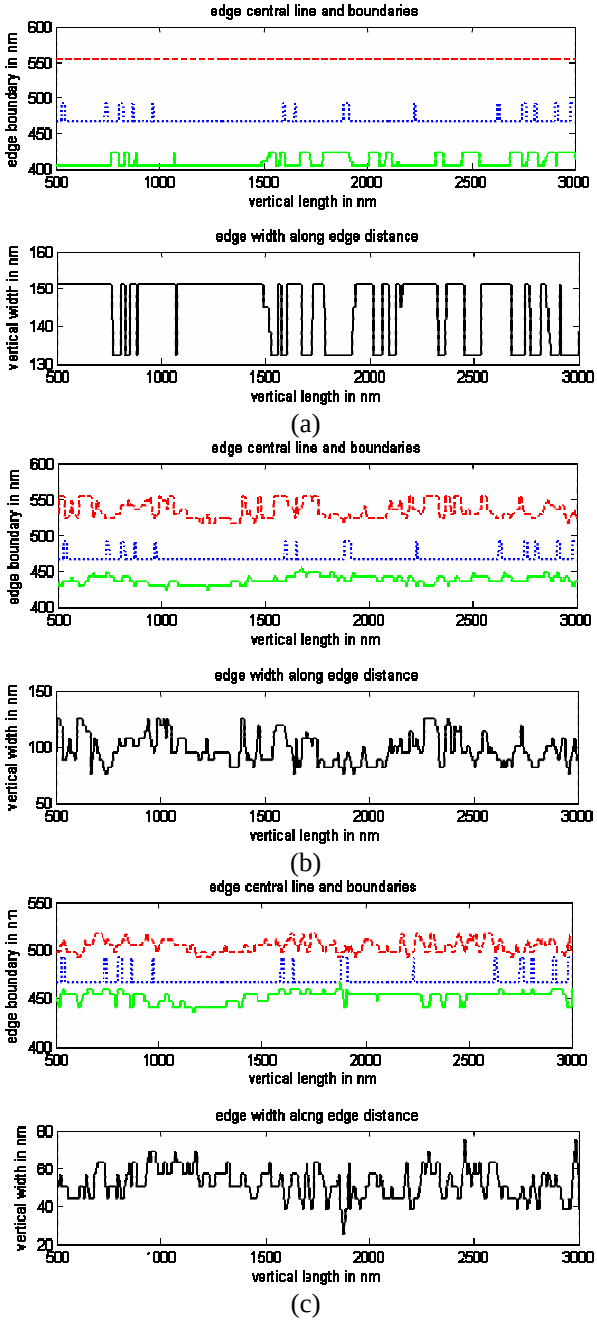

Fig. 3. The plots show the upper (dash) and lower (dot) edge boundaries and the maximum intensity line (solid) as well as the edge width along the edge distance in nm. Edge boundaries are found by thresholding based on de-noised image, for threshold value of (a) 0.2, (b) 0.6, and (c) 0.8. With increasing threshold value, edges appear well separated and defined. The edge boundaries also appear smoother due to the de-noising operation in the intensity direction.

The results of sigma and correlation coefficient calculations are shown in Table I. It is noted that the sigma value relative to the linear fitting of edge boundaries decreases at small threshold values, but starts to increase again when the edge width significantly shrinks and the calculation of the sigma value starts to reflect surface variations. The desirable threshold value (0.6) is highlighted in Table I. The absolute

TABLE I
CHARACTERIZATION RESULTS FOR EDGE BOUNDARIES FOUND BY THRESHOLDING ON DENOISED IMAGE

Threshold Value	Edge width (nm)	Sigma (nm)	Absolute value of correlation coefficient between upper and lower boundaries
0.2	145.6 ± 8.5	7.8	N/A
0.5	119.6 ± 10.2	11.1	0.1246
0.6	96.0 ± 12.5	12.8	0.1162
0.7	74.2 ± 7.8	8.1	0.1134
0.8	51.0± 7.9	8.7	0.1779
0.9	23.4±21.3	17.0	0.6059

TABLE II
CHARACTERIZATION RESULTS FOR EDGE BOUNDARIES FOUND BY THRESHOLDING ON ORIGINAL IMAGE

Threshold Value	Edge width (nm)	Sigma (nm)	Absolute value of correlation coefficient between upper and lower boundaries
0.2	145.9 ± 7.4	7.6	0.0413
0.5	125.1±13.2	12.9	0.0056
0.6	111.6 ± 13.7	13.9	0.0628
0.7	88.7 ± 14.1	14.7	0.1343
0.8	59.1 ± 10.8	11.7	0.1806
0.9	29.5 ± 15.1	14.1	0.1301

correlation coefficient between the two boundaries is generally small, indicating that they are independent from each other as expected. We also note that this coefficient becomes significantly high when the threshold value is 0.9, a strong indication that the edges become highly correlated between two smoothed parallel boundary lines due to over-smoothing.

Table II shows that the edge width and the sigma values are much higher than the ones corresponding to the de-noised image, indicating the increased uncertainty for this case. This uncertainty stems from the artifacts due to the imaging process and also includes the high-frequency components of the edge itself. It is noted that the edge search region is determined visually here. It is difficult to see if it covers the whole edge region or it already includes a region associated with the other edge.

In addition to the characterization of a single edge, behavior of a pair of adjacent edges can also be studied. This analysis will show the degree of parallelism and the correlation between the edges in more detail, and can be used as a basis for quantifying the performance of the fabrication process. Here, we use the slope of the line obtained by a linear fitting of the maximum intensity profile and compare the slope values for each edge. Pair edge boundaries are determined for the threshold value of 0.6. In Table III, we indicate the slopes of the maximum intensity linear fit for each edge, and the correlation coefficient of the maximum intensity between two

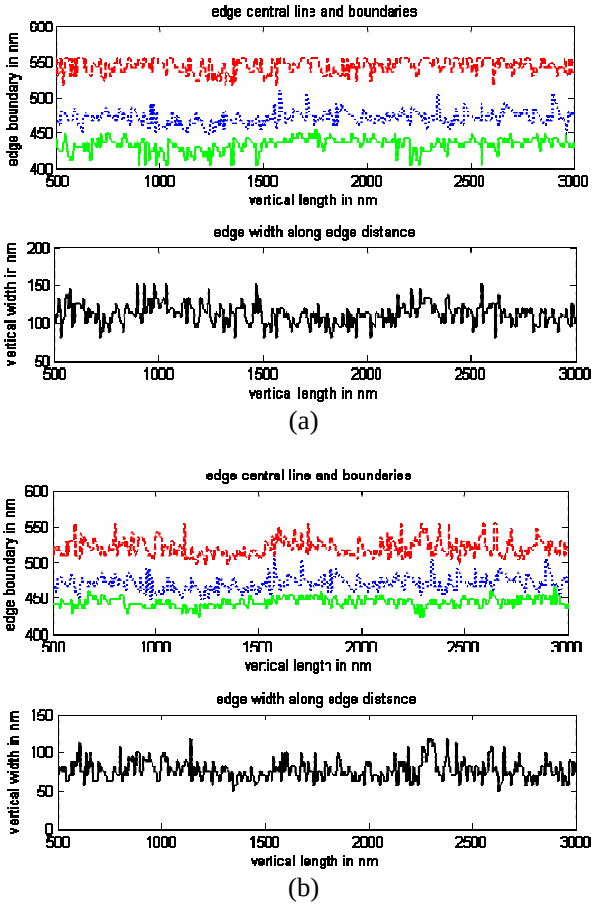

Fig. 4. Edge boundaries and width at automatically generated threshold values. (a) At threshold value of intensity mean + σ (0.6290), (b) at threshold value of intensity mean + 2σ (0.7617).

edges. The slope values show that two linear fits based on the maximum intensity of each edge are almost parallel and they are independent of each other, and this indicates a successful patterning of the lines.

C. Edge Detection by Wavelet Decomposition and LER Characterization

Wavelet decomposition can efficiently separate an image into an approximation image (smoothed sub-image) and a detail image (sub-image with high-frequency details). The low- frequency part mainly contains the edge features and the background, and the high-frequency part typically results from the surface roughness and imaging artifacts. As wavelet decomposition is performed at each level, the high-frequency components in the image are sequentially removed. The remaining approximation part of the image becomes smoother as the decomposition progresses. The suitable approximation we are looking for shall eliminate the random features, but retain the edge and the background features. To facilitate this decision, we need a performance metric (i.e., an objective function). One possible metric is the Shannon entropy which calculated for the approximation image at each decomposition level. Shannon

TABLE III
CHARACTERIZATION RESULTS FOR PAIR EDGES

	Slope 1	Slope 2	Absolute value of correlation coefficient
De-noised image	0.0000	0.0000	0.0439
Original image	0.0008	0.0029	0.0800
Wavelet based	0.0008	0.0029	0.0800

TABLE IV
SHANNON ENTROPY FOR WAVELET APPROXIMATION SUB-IMAGE AT EACH LEVEL

Decomposition level	1st	2nd	**3rd**	4th	5th
Shannon entropy (1.0×10^4)	7.263	7.286	**7.226**	7.739	8.295

TABLE V
CHARACTERIZATION RESULTS FOR EDGE BOUNDARIES FOUND BY WAVELET DECOMPOSITION

Threshold Value	Edge width (nm)	Sigma (nm)	Absolute value of correlation coefficient between upper and lower boundaries
0.496(μ)	130.9 ± 12.4	12.2	0.0239
0.629(μ+σ)	111.6 ± 13.7	13.9	0.0628
0.762(μ+2σ)	76.5 ± 12.8	13.3	0.1071
0.894(μ+3σ)	34.1 ± 12.4	12.7	0.0344

is a measure of the efficiency of a given expansion over all basis functions [15]. It yields the distance between a basis and a function and enables the search for a smallest entropy spatial decomposition of a signal (image). In other words, it establishes a cost function for the information content of a signal (image) at different levels of decomposition using special basis functions. Its minimum is therefore sought for locating the optimal wavelet decomposition. For the image under consideration here, the minimum value is obtained at the 3rd level (Table IV) using the *db*3 wavelet function. This implies that further decomposition will introduce variance of the wavelet base function to the approximation part, which is not the information from the original image. Thus, the 3rd level wavelet approximation is used to find the edge searching region in this study.

By searching for local minima in the direction perpendicular to the edge, the edge search region can be automatically (without visual bias) generated. This reduces the noise impact on the original image. At the same time, the approximation sub-image yields an average intensity along the separating line between two adjacent edges. A suitable threshold value is required to sufficiently separate two adjacent edges and also to maintain the edge boundary deviation in edge roughness characterization. Statistics from

the sub-image with high-frequency component describe intensity deviation on the surface. To illustrate, we chose different threshold values

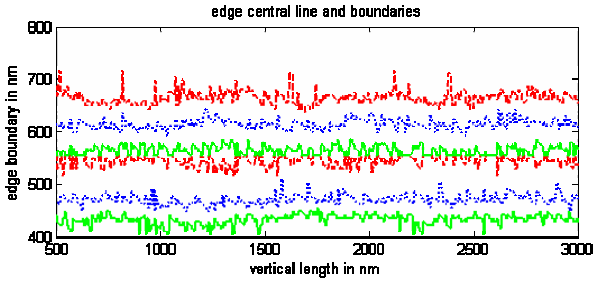

Fig. 5. Pair edge image and its boundaries decided by wavelet decomposition at threshold value of intensity mean +δ (0.6290).

based on the mean of the approximation sub-image and the standard deviation of the detail sub-image. Edge boundaries and characterization results at different threshold values are summarized in Figure 4 and Table V.

Results in Table V show a similar trend as in Table II. The maximum edge roughness is obtained at 0.6290 (now quantified as one standard deviation), where edges are well-separated and the edge width has not significantly decreased. As opposed to other techniques, with wavelet decomposition, the choice of the threshold is set by uniformly-defined characteristics of the image itself, i.e., the standard deviation of the detail image and the mean of the approximation sub-image, where the former characterizes the density variance of the image and the latter represents the backbone of the edge studied.

Pair edge boundary and characterization based on denoised wavelet decomposition is shown in Figure 5 and Table III. The threshold value is different from the one obtained from the original image, but the results are similar, since only the maximum intensity lines are considered. Again, the weak correlation between two paired edges is expected for a successful fabrication process.

V. Conclusion

Edge detection and characterization based on wavelet decomposition provide systematic evaluation of the superimposed edge search region and of the threshold value, which are both intrinsic properties of the image itself. The defined parameter *sigma* reveals the edge roughness at the corresponding threshold value. Based on the threshold calculation described in this paper, *sigma* yields a value close to the maximum edge roughness and therefore eliminates the need for visual evaluation. We demonstrated that wavelets provide an analytical framework to define the edge searching region, and minimize the need for subjective decisions in characterizing the line edge roughness. Our results indicate that this method can be a powerful tool for nanometer-scale edge detection and characterization for fabrication of advanced microelectronic devices and other nanometer-scale structures.

Appendix

A 1-D signal *f(t)* can be decomposed using the wavelet transformation and a family of real orthonormal bases $\psi_{j,k}(t)$, which are generated from a kernel function $\psi(t)$:

$$\psi_{j,k}(t) = 2^{-j/2}\psi(2^{-j}t - k) \tag{2}$$

where j and k are integers, representing the dilations and translations. The wavelet coefficients of the signal *f(t)* can be calculated by the inner product,

$$a_{j,k} = \left\langle f(t), \psi_{j,k}(t) \right\rangle = \int f(t)\psi_{j,k}(t)dt \tag{3}$$

Another basis function, the scaling function ($\phi(t)$), is needed in addition to the mother wavelet $\psi(t)$ to establish the multiresolution characteristics of the wavelet decomposition. $\phi(t)$ can be expressed in terms of a weighted sum of shifted $\phi(2t)$ as:

$$\phi(t) = \sqrt{2}\sum_n l(n)\phi(2t - n) \tag{4}$$

where $l(n)'s$ are the coefficients of a low-pass filter in the fast Discrete Wavelet Transform (DWT) calculation [5]. The mother wavelet $\psi(t)$ and the scaling function $\phi(t)$ are related through the expression,

$$\psi(t) = \sqrt{2}\sum_n h(n)\phi(2t - n) \tag{5}$$

where $h(n)'s$ are coefficients now corresponding to a high-pass filter. Two filters are related through the expression,

$$h(n) = (-1)^n l(1 - n) \tag{6}$$

While the mother wavelet $\psi(t)$ represents the detail (high-frequency) elements of the signal, the scaling function $\phi(t)$ captures the approximation (low-frequency) component of the signal. In the actual calculation, $l(n)$ and $h(n)$ are more commonly used to perform the transform as

$$\begin{aligned} c_{j,k} &= \sum_n c_{j-1,k}\, l(n - 2k) \\ d_{j,k} &= \sum_n c_{j-1,k}\, h(n - 2k) \qquad \text{for } j = 1,2,...J \end{aligned} \tag{7}$$

Here, the coefficients $c_{0,n}$ represent the original signal. The coefficients $c_{j,k}$ correspond to the smoothed approximation (low-frequency) part of the decomposed signal at *j*th level, and are usually called the *approximation coefficients*. The coefficients $d_{j,k}$ correspond to the detail (high-frequency) part of the decomposed signal at *j*th level, and are usually referred to as the *wavelet (detail) coefficients*.

This decomposition halves the spatial resolution since only half the number of samples now characterizes the entire signal. However, this operation doubles the frequency resolution, since the frequency band of the signal now spans

only half the previous frequency band, effectively reducing the uncertainty in the frequency by half. The above procedure can be repeated for further decomposition levels. At each level, the filtering and sub-sampling will result in half the number of samples (and hence half the spatial resolution) and half the frequency band spanned (and, hence, doubling the frequency resolution).

In moving from 1D to 2D wavelet transform, the rows and columns of the data matrix (*x* and *y* coordinates) that represent the image are treated as independent. Therefore, the 2D filters become the tensor products of their 1D counterparts [16]:

$$\phi^{LL}(x,y)=\phi(x)\phi(y) \quad \phi^{LH}(x,y)=\phi(x)\psi(y)$$

$$\phi^{HL}(x,y)=\psi(x)\phi(y) \quad \phi^{HH}(x,y)=\psi(x)\psi(y) \qquad (8)$$

Applying the filters to the image data ($M \times N$ array) results in

$$f_L(x,y)=\frac{1}{N_l}\sum_{i=0}^{N_l-1} l[i]\, f((2x+i) \bmod N, y)$$

$$f_H(x,y)=\frac{1}{N_h}\sum_{i=0}^{N_h-1} h[i]\, f((2x+i) \bmod M, y) \qquad (9)$$

for $x=0,1,2,...,(M/2)-1$ and $y=0,1,2,...,(N-1)$. Here, N_l and N_h represent the support length of the low- and high-pass filters, respectively. And furthermore,

$$f_{LL}(x,y)=\frac{1}{N_l}\sum_{i=0}^{N_l-1} l[i]\, f_L(x,(2y+i) \bmod N)$$

$$f_{LH}(x,y)=\frac{1}{N_h}\sum_{i=0}^{N_h-1} h[i]\, f_L(x,(2y+i) \bmod N)$$

$$f_{HL}(x,y)=\frac{1}{N_l}\sum_{i=0}^{N_l-1} l[i]\, f_H(x,(2y+i) \bmod N) \qquad (10)$$

$$f_{HH}(x,y)=\frac{1}{N_h}\sum_{i=0}^{N_h-1} h[i]\, f_H(x,(2y+i) \bmod N)$$

for $x=0,1,2,...,(N/2)\ldots-1$ and $y=0,1,2,...,(N/2)-1$.

A schematic for a one-level decomposition of a 2D image is shown in Figure 6(a). A high-pass and a low-pass filter are applied to the image in the *x*-direction (across the row of the matrix), and the results are down-sampled by deleting every other column. This results in two images of approximately half size of the original, one containing high frequency components of the rows, f_H, and the other containing low frequency components, f_L. These two images are then each filtered down the columns using high-pass and low-pass filters and down-sampling the results along the rows (deleting every other row). The resulting four images are approximately one-fourth the size of the original image.

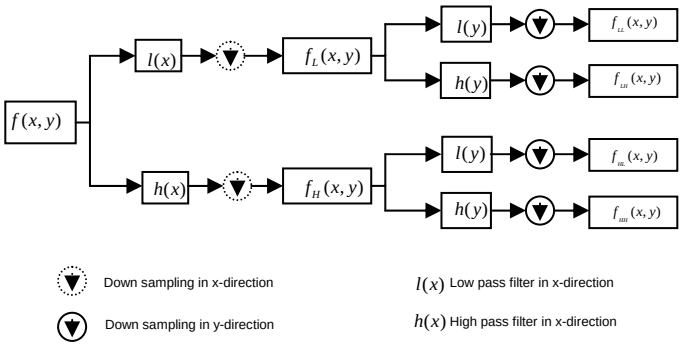

(a)

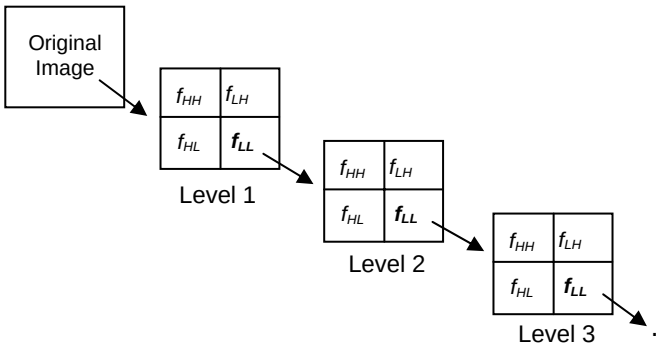

(b)

Fig. 6. Schematic of one-level, 2D wavelet decomposition (a) and the multiresolution strategy for image decomposition (b).

The sub-images f_{LL}, f_{LH}, f_{HL} and f_{HH} represent the smoothed approximation, the horizontal detail, the vertical detail and the diagonal detail sub-images respectively (Figure 6(b)). The process can be iterated on the smoothed approximation sub-image to obtain the decomposition in the next level.

ACKNOWLEDGMENT

The authors gratefully acknowledge Jerald Britten of Lawrence Livermore National Laboratory (LLNL) for providing the grating sample for analysis, and Phillip Hailey and Bassem El Dasher (LLNL) for SEM imaging.

REFERENCES

[1] E. Gogolides, V. Constantoudis, and G. P. Patsis, "A review of line edge roughness and surface nanotexture resulting from patterning processes" Microelectronic Engineering, vol. 83, pp. 1067-1072, Apr.-Sep. 2006.

[2] S. Winkelmeier, M. Sarstedt, M. Ereke, M. Goethal, and K. Rons, "Metrology method for the correlation of line edge roughness for different resists before and after etch," Microelectronic Engineering, vol. 57-58, pp. 665-672, 2001.

[3] A. Yamaguchi, R. Steffen, R. Kawada, T. Iizumu, and A. Sugimoto, "A discussion on how to define the tolerance for line-edge or linewidth roughness and its measurement methodology," IEEE Trans. On Semiconductor Manufacturing, vol. 20, pp. 549-555, Nov. 2007.

[4] G. P. Patsis, V. Constantoudis, A. Tserepi, E. Gogolides, and G. Grozev, "Quantification of line-edge roughness of photoresists. I. A comparison between off-line and on-line analysis of top-down scanning electron

microscopy images," J. Vac. Sci. & Tech. B, vol. 21, pp. 1008-1018, 2003.
[5] G. Strang, and T. Nguyen, *Wavelets and Filter Banks*. Wellesley, MA; Wellesley-Cambridge Press, 1996.
[6] M. Carmichael, A. Maksumov, R. Vidu, A. Palazoglu, and P. Stroeve, "Using Wavelets to Analyze AFM Images of Thin Films: Surface Micelles and Supported Bilayers," Langmuir, vol. 20, pp. 11557-11568, 2004.
[7] W. S. Choi, M. T. Lim, and B. Kim, "Prediction of etch profile uniformity using wavelet and neural network," Int. J. of Control Automation and Systems, vol. 2, pp. 256-262, 2004.
[8] B. Kim, W. Ko, and S. S. Han, "Neural network recognition of scanning electron microscope image for plasma diagnosis," Lecture Notes in Artificial Intelligence, vol. 4099, 350-357 2006.
[9] K. Nakamae, M. Chikasa, and H. Fujioka, "Estimation of electron probe profile from SEM image through wavelet multiresolution analysis for inline SEM inspection," Image and Vision Computing, vol. 25, 1117-1123, 2007.
[10] T. Yamaguchi, K. Yamazaki, M. Nagase, and H. Namatsu, "Line-edge roughness: Characterization and material origin," Japan. J. Appl. Phys., vol. 42, 3755-3762, 2003.
[11] V. Constantoudis, G. P. Patsis, A. Tserepi, and E. Gogolides, "Quantification of line-edge roughness of photoresists. II. Scaling and fractal analysis and the best roughness descriptors," J. Vac. Sci. & Tech. B, vol. 21, pp. 1019-1026, 2003.
[12] V. Constantoudis, G. P. Patsis, and E. Gogolides, "Photoresist line-edge roughness analysis using scaling concepts," J. Microlithography Microfabrication and Microsystems, vol. 3, pp. 429-435, 2004.
[13] A. Yamaguchi, and O. Komuro, Jpn. J. Appl. Phys., 42, 3763 (2003).
[14] S. G. Mallat, "A theory for multiresolution signal decomposition –The wavelet representation," IEEE Trans. Pattern Analysis and Machine Intell., vol. 11, pp. 674-693, 1989.
[15] R. R. Coifman, and M. V. Wickerhauser, "Entropy based algorithms for nest basis selection," IEEE Trans. on Inf. Theory, vol. 8, pp. 713-718, 1992.
[16] DM. Tsai, and B. Hsiao, "Automatic surface inspection using wavelet reconstruction," Pattern Recognition, vol. 34, pp. 1285-1305, 2001.

Wei Sun received her M.Sc. in management science from University of Science and Technology of China, and Ph.D. in chemical engineering from University of California, Davis, USA. She is currently an associate professor in Beijing University of Chemical Technology, Beijing, China. Her research interests include process monitoring, image processing, and engineering applications of wavelet transform.

Jose A. Romagnoli received his BS degree (Chemical Engineering) from Universidad Nacional del Sur, Argentina and PhD (Chemical Engineering) from the University of Minnesota, USA. He currently holds the Gordon A. and Mary Cain Endowed Chair in the Department of Chemical Engineering, Louisiana State University, USA. He is also the M. Gautreaux /Ethyl Chair Professor at the same university and the Director of the Process Systems Engineering Laboratory.

Dr. Romagnoli was awarded the Centenary Medal of Australia by the Prime Minister of Australia for contributions to the field of Chemical Engineering (2003). He is a fellow at the Australian Academy of Technological Sciences and Engineering for contributions to the field of Process Systems Engineering (1999). He is a fellow of the Institution of Engineers, Australia (1996) and the author of two books and has numerous writings and publications.

Joseph Tringe (M'00) received his A.B. in Physics from Harvard University and his Ph.D. in Materials Science from Stanford University.

He served in the Air Force from 1999 to 2003, assigned to the Space Vehicles Directorate of the Air Force Research Laboratory at Kirtland AFB, New Mexico, where he led the Electronics Foundations group and studied MEMS, nanostructured devices and radiation effects. He has been with Lawrence Livermore National Laboratory since 2003, where his research interests include advanced sensors and power sources.

Sonia E. Létant was born in Annecy, France, in 1973. She attended the Joseph Fourier University in Grenoble where she received a Masters degree in Materials Science in 1995 and a Ph.D. in Physics in 1998 for her work on energy and charge transfer in confined porous semiconductors using the newly discovered nano-porous silicon. She conducted postdoctoral research as a Lavoisier Fellow, between 1998 and 2001, in the Department of Chemistry and Biochemistry at the University of California, San Diego, where she worked on surface functionalization and transduction schemes for chemical and biological sensing.

She joined the Chemistry and Materials Science Directorate at Lawrence Livermore National Laboratory in 2001 as a directorate postdoctoral fellow. She was appointed as a Physicist in 2002, and became the Scientific Capability Leader for the Functional Materials and Molecular Structures group in 2006. Her current research focuses on the design, fabrication, and characterization of multi-functional nano-structured materials and platforms for separation and sensing. She holds 2 US patents and her work has been published in Nature Materials, Advanced Materials, Nanoletters, Small, Applied Physics Letters, Physical Review Letters and the Journal of the American Chemical Society.

Dr. Létant was the recipient of an M.E.S.R. fellowship from the French Department of Superior Education and Research from 1995 to 1998 and she was a Lavoisier postdoctoral fellow between 1998 and 2001.

Pieter Stroeve was born in the Netherlands. He received the B.S. in Chemical Engineering in 1967, at the University of California, Berkeley, CA, and the M.S. and Sc. D. in Chemical Engineering at the Massachusetts Institute of Technology in 1969 and 1973, respectively. Currently he is a Professor of Chemical Engineering at the Department of Chemical Engineering and Materials Science, University of California Davis, CA.

He is the former Co-Director of the NSF Center on Polymer Interfaces and Macromolecular Assemblies (CPIMA). He conducts research in nanotechnology, macromolecular self-assembly, image analysis, membrane separations and colloid and interface science.

Ahmet Palazoglu received his B.S. and M.S. degrees in chemical engineering from Middle East Technical University, Turkey and Bogazici University, Turkey, in 1978 and 1980, respectively. He received his PhD in chemical engineering in 1984 from Rensselaer Polytechnic University in Troy, NY, focusing on robust control design.

He has joined the Chemical Engineering and Materials Science Department at University of California, Davis in 1984, and been there since that time. He has over 100 publications and two co-authored books, Introduction to Process Control (Boca Raton, FL: Taylor & Francis, 2006) and Chemical Process Performance Evaluation (Boca Raton, FL: Taylor & Francis, 2007). His research areas include process control and monitoring, nonlinear systems, statistical modeling in biological and environmental systems as well as image analysis using wavelets.

Dr. Palazoglu received the Tarik Somer Award from Middle East Technical University, Turkey in 2005.